



A DFT study of H₂S adsorption and sensing on Ti, V, Cr and Sc doped graphene surfaces

Ömer Faruk Tunali¹ · Numan Yuksel² · Gökhan Gece¹ · M. Ferdi Fellah²

Received: 10 November 2023 / Accepted: 6 December 2023 / Published online: 3 January 2024
© The Author(s), under exclusive licence to Springer Science+Business Media, LLC, part of Springer Nature 2024

Abstract

Finding cost-effective and sustainable methods for the removal of hydrogen sulfide (H₂S), a highly toxic gas released as a byproduct in many industrial activities, is crucial for environmental health. In this study, the adsorption and electronic sensor properties of Ti, V, Cr and Sc doped graphene nanosheets (GN) for H₂S molecule have been investigated using Density Functional Theory (DFT) method. The WB97XD method with 6-31G(d,p)/LanL2DZ basis sets have been utilized in DFT calculations. The charge distribution indicates that the charge transfer occurred between metal doped graphenes and H₂S. DFT calculations of H₂S molecule adsorption on Ti, V, Cr and Sc doped graphenes demonstrate that the ability to adsorb H₂S molecule. The obtained adsorption energy (ΔE) values vary in the range of -54.4 to -71.0 kJ/mol. Furthermore, the electrical conductivity of the Cr doped graphene nanosheet (Cr-GN) changed due to the change in the HOMO–LUMO gap ($\Delta E_g = 24.8$ kJ/mol). This result indicates that the Cr-GN structure is a potential candidate as an electronic sensor for H₂S molecule at room temperature. Through methods like DFT, which are cost-effective and highly compatible with experimental results, predicting suitable adsorbents, understanding their properties, and enhancing them are expected to make substantial contributions to the industrial-scale production of these materials in terms of cost and accuracy in the future.

Keywords DFT · Graphene · Metal doping · Hydrogen sulfide · Adsorption · Sensor

Introduction

The advancement in agriculture and industry has augmented the environmental toxic load, attributable to various products employed in industrial processes, including mercury (Hg), pesticides, electronic devices, and batteries [1]. Toxic gas emissions, which are very dangerous for nature, are usually caused by industrial production wastes. These gases are also a significant threat to human life. Because even a very small amount of exposure to some gases can cause permanent damage to human health. For example, H₂S which occurs naturally or as a by-product in factory production, is dangerous even at the ppm level. According to OSHA (Occupational Safety and Health Administration) criteria, the safe H₂S level was determined as 20 ppm during the

daily work (6–8 h) [2, 3]. Therefore, removal of H₂S is a necessary process. Especially in industry, it causes corrosion in transport lines and poisoning of any catalysts even at low levels [4].

Known to have serious effects on the eyes and respiratory tract in the range of 20–50 ppm [5]. Moreover, H₂S exposure in the range of 100 to 500 ppm for 1 h can cause serious damage such as respiratory paralysis and loss of consciousness, while at higher levels it can cause sudden respiratory arrest and death [5, 6]. As a result, H₂S gas in the environment should be detected with appropriate methods, with high accuracy and quickly [6]. It is worth emphasizing that H₂S exhibits a higher density than air, leading to its propensity for accumulation within confined environments. Consequently, the utmost vigilance and implementation of appropriate protocols for H₂S mitigation are imperative for individuals operating in subterranean workplaces, man-holes, and comparably inadequate ventilation settings. Thus far, comprehensive investigations have been conducted to explore diverse desulfurization methodologies encompassing membrane separation, adsorption, catalytic oxidation, and distillation processes [7, 8]. In recently, a prominent

✉ Numan Yuksel
n.yuksel@btu.edu.tr

¹ Department of Chemistry, Bursa Technical University, Mimar Sinan Campus, 16310 Bursa, Turkey

² Department of Chemical Engineering, Bursa Technical University, Mimar Sinan Campus, 16310 Bursa, Turkey

research trend has emerged focusing on the utilization of materials possessing at least one dimension within the range of 1 to 100 nm to construct sensors characterized by high sensitivity and economical attributes. Nanomaterials (NMs) are recognized as optimal platforms for applications involving gas adsorption owing to their remarkable surface area to volume ratio and distinctive hollow configuration. Increased surface area facilitates the augmentation of active sites for molecular interactions, thereby resulting in heightened chemical reactivity and enhanced adsorption capacities. This characteristic confers a distinctive advantage in gas adsorption applications, as nanomaterials demonstrate exceptional proficiency in the efficient sequestration and steadfast retention of gas molecules upon their surfaces [9]. Over the past few decades, carbon-based nanomaterials (C-NMs) have garnered significant attention due to their extraordinary electronic, magnetic, and optical characteristics, alongside their chemical adaptability and biocompatibility [10–14].

For instance, carbon-based organic polymers modified with heteroatoms such as S, P, O, N are favored due to their advantages in surface area, porosity, and cost-effectiveness [15]. Nanotubes [16], activated carbons [17–20], and graphene [21, 22] are among the carbon-based materials that have demonstrated their efficacy as adsorbents and catalyst enhancers. In general, graphene nanoparticles (Gnp) can be toxic to living organisms by bypassing physiological barriers to varying degrees. Different application methods and routes of entry, along with varying tissue distribution and clearance, can determine the degree of toxicity of Gnp. For instance, graphene oxide (GO) can interfere with the normal physiological functions of vital organs, leading to acute inflammatory responses and chronic damage [23]. Nevertheless, in industrial fields, graphene has emerged as an exceptionally promising material in various applications, especially in gas sensors, due to its outstanding mechanical properties, electrical conductivity, and thermal conductivity. Graphene, a two-dimensional material comprising a monolayer of carbon atoms organized in a hexagonal lattice, has garnered considerable interest since its experimental synthesis in 2004 [24–26]. Its unique atomic structure and remarkable properties make it a compelling candidate for gas sensing applications, where its high sensitivity and selectivity are crucial factors to consider. The extensive research conducted on graphene-based gas sensors underscores its potential in advancing the field and addressing various sensing challenges [3]. In recent years, graphene has been the subject of numerous research as a promising adsorbent for H₂S, a prevalent industrial pollutant [27, 28]. Additionally, it can undergo uniform doping with metals/non-metals or relevant functional groups, thereby enhance its adsorption capability [29–35]. Natan and co-workers, the adsorption mechanism of H₂S molecules on pristine

and Pt-decorated graphene sheets was investigated using density functional theory calculations based on local density approximation and generalized gradient approximation methods. It has been found that graphene sheets with a Pt atom on each side can stably bind up to seven H₂S molecules, each exhibiting the desired binding energy [32]. In another study, the adsorption mechanism, electrical conductance, and binding energy of H₂S gas on pure graphene sheets (GS) as well as Cu-decorated and CuO-decorated GS were investigated. The findings revealed that the CuO-GS structure exhibited a higher binding energy with H₂S compared to Cu-GS and GS, and important orbital hybridization was observed between H₂S and Cu-GS as well as H₂S and CuO-GS, whereas no hybridization was detected between H₂S gas and GS [36]. The adsorption performance of graphene structures exposed to H₂S and CH₄ molecules was investigated. It was found that Ni-doped graphene (Ni-G) structures exhibited critical effectiveness in H₂S adsorption. Combining vacancy defect graphene (DG) structures with Ni-doped graphene showed promise as a viable option for H₂S gas detection [37]. In the literature, it was observed that a graphene sheet decorated with Ni atoms serves as a more favorable adsorbent for H₂S molecules compared to undecorated graphene or graphene decorated with BeO or ZnO [38]. Due to differences in chemical potentials, the geometric configuration and chemical bonding of a single metal atom dopant on the support produce unique electronic structures that cause charge transfer between the metal atoms and the support. When acting as active centers, single metal atoms doped into carbon-based materials with distinct and atomically distributed metal atoms on supports can maximize metal utilization efficiency. Carbon-based materials doped with a single metal atom can also be used as a simple model system to compare theoretical predictions with experimental results [39]. According to Qiu et al. atomic nickel doped graphene exhibits good HER activity with a minimal over potential and Tafel slope in an acidic electrolyte when compared to commercial Pt/C and other reported catalysts. It turns out that the strong interaction between the Ni substituents in the carbon framework is the cause of this performance [40]. In a review published by Sun et al. it was stated that element doping into the carbon matrix can reduce residual stress, increase adhesion strength, and improve tribological, corrosion resistance, hydrophobicity, biocompatibility and optical properties [41].

In this study, the adsorption and detection of H₂S gas were conducted on graphene surfaces doped with Ti, V, Cr, and Sc metal atoms at room temperature, some of which have not been encountered in the literature before. In addition, the comparison of results aimed to identify the atom that provides the most efficient outcomes when combined with graphene.

Computational method

In this study, DFT [42] calculations were used via Gaussian 09 software [43] to obtain optimized geometries and electrical properties. As the method, the WB97XD (including distribution) hybrid method was used, which takes into account the effects of exchange and correlation [44]. The WB97XD functional augments the WB97X functional with a parameterized classical dispersion term and a van der Waals correction [45]. Additionally, dipole correction was not taken into account in the DFT calculations because its effect is less significant (between 3.8 and 6.7 kJ/mol) [46]. In this study, a graphene sheet structure with 73 carbon atoms was used and a cluster model was created by attaching 21 hydrogen atoms to the ends of the bonds between the free carbon atoms in the sheet. There are 27 hexagonal honeycomb rings in the structure. The graphene structure used in this study is large enough. Smaller graphene clusters have been used in the literature [47]. All atoms were kept at a relaxed state throughout the theoretical computations. Metal atom was replaced with a carbon atom in the center of the graphene structure to form Ti, V, Cr, and Sc doped graphene sheets. The 6-31G (d,p) basis set was employed for carbon, oxygen, hydrogen, and sulfur atoms, whereas LanL2DZ was employed for Ti, V, Cr, and Sc atoms. In DFT calculations, first of all, Spin Multiplicity (SM) calculations are made and optimized geometries for the most stable SM value are obtained. Optimized geometries were used to obtain the equilibrium geometry (EG) and adsorption energies. The energy difference values account for the zero-point energy (ZPE) corrections. The following equations were utilized to calculate the energy values for H₂S adsorption on Ti, V, Cr, and Sc doped graphene structures:

$$E = E_{\text{electronic}} + \text{ZPE} + E_{\text{vibrational}} + E_{\text{rotational}} + E_{\text{translational}} \quad (1)$$

$$H = E + RT \quad (2)$$

$$G = H - TS \quad (3)$$

Here, E is the total of the thermal, electronic, and zero-point energies, H is the enthalpy, G is the Gibbs free energy, S is the entropy and T is the absolute temperature (298.15 K). The values of the relative adsorption energy (ΔE), enthalpy (ΔH) and Gibbs free energy (ΔG) were determined using Eq. (4).

$$\Delta(E/H/G) = (E/H/G)_{\text{System}} - [(E/H/G)_{\text{Adsorptive}} + (E/H/G)_{\text{Cluster}}] \quad (4)$$

Here, System is H₂S adsorbed metal doped graphene, Adsorptive is adsorbing molecule (H₂S) and cluster is metal doped graphene structures. For the theoretical calculations used in this study, the convergence criteria are 12×10^{-4} rad

for gradients of root-mean-square (rms) displacement, 18×10^{-4} bohr for maximum displacement, 3×10^{-4} hartree/radian for rms force, and 45×10^{-5} hartree/bohr for maximum force. Additionally, the RMS change in the density matrix and the maximum change in the density matrix had SCF convergence criterion of 1×10^{-8} and 1×10^{-6} , respectively. Natural Bond Orbital (NBO) atomic charges of atoms [48] has been found by using the NBO population analysis. In addition, the graphs for Reduced Density Gradient (RDG) scatter graphs and isosurfaces of RDGs, Total Density of States (TDOS) and Partial Density of States (PDOS) were obtained by using Multiwfn software [49].

Results and discussions

For the adsorption of H₂S gas on metal-doped graphene structures by DFT method, firstly, the graphene sheet was modeled as a cluster and doped with metal atoms. Initially, pristine graphene structure was optimized and H₂S adsorption was performed. The aim here is to see the effects of metal doping and graphene support material on adsorption. Figure 1 shows the optimized geometries for pristine graphene and H₂S adsorbed pristine graphene structures. H₂S adsorption energies of pristine graphene; ΔE , ΔH

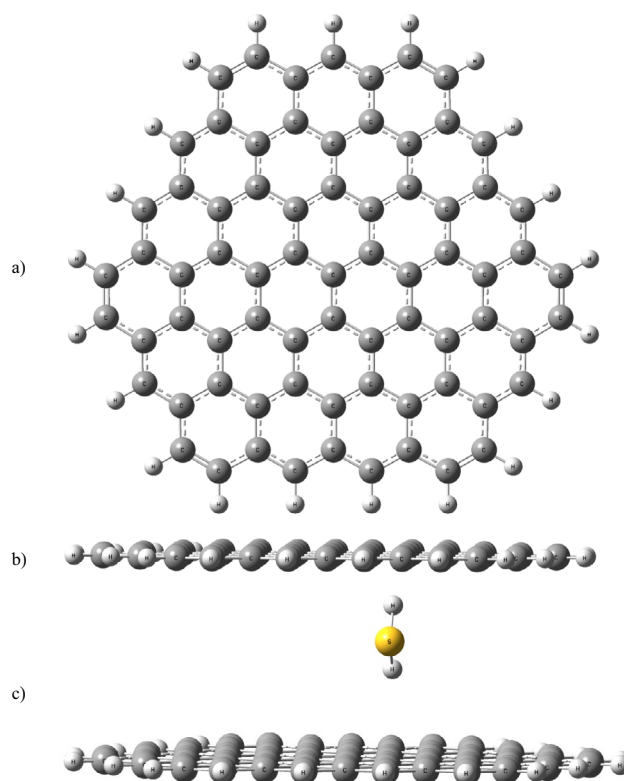


Fig. 1 **a** Top view and **b** side view of the optimized pristine graphene structures, and **c** H₂S adsorbed pristine graphene

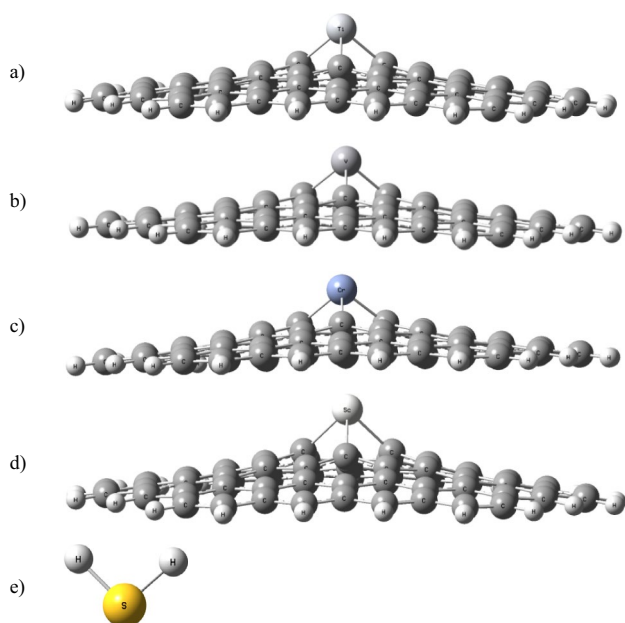
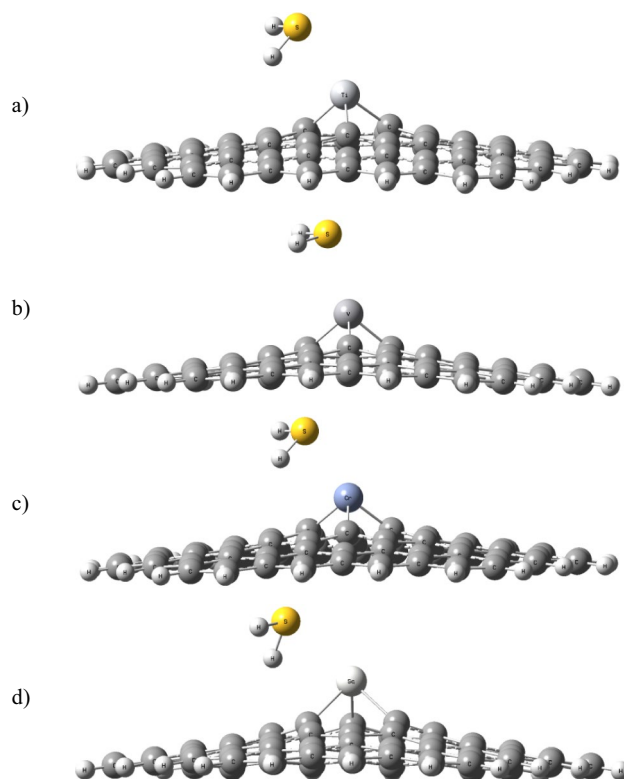
Table 1 Determined SM values and of metal doped graphenes and H₂S molecule

Structure	SM
Ti-graphene	doublet
V-graphene	triplet
Cr-graphene	quartet
Sc-graphene	singlet
H ₂ S	singlet

and ΔG values were calculated as -9.0, -11.5 and 18.4 kJ/mol, respectively. A metal atom was replaced with a central carbon atom. The SM values of the structures and the H₂S molecule are given in Table 1. Also, the formation energies (E_F) of metal-doped graphene structures were calculated according to Eq. (5) [50, 51]. The E_F value for all structures was calculated as ~ -7.5 eV. Accordingly, the fact that the formation energies remain negative indicates that metal-doped graphene remains stable.

$$E_F = \left(\frac{E_{\text{System}} - x.E_C - y.E_H - z.E_M}{N} \right) \quad (5)$$

Here, E_{System} is thermal energy of metal-doped graphene, x , y and z are number of C, H and metal atoms respectively. N is the number of total atoms. E_C , E_H and E_M are the thermal energies of C, H and metal atoms respectively. The optimized geometry of the H₂S molecule and metal doped graphenes are shown in Fig. 2. For the optimized H₂S molecule, the H–S bond length was calculated as 1.34 Å and the H–S–H bond angle as 93.0°. In the literature, these values were reported as 1.38 Å and 94°, respectively, by the B3LYP

**Fig. 2** The optimized geometries of **a** Ti, **b** V, **c** Cr and **d** Sc doped graphenes and **e** H₂S molecule**Fig. 3** Optimized geometries of H₂S adsorbed on **a** Ti, **b** V, **c** Cr and **d** Sc doped graphenes

(including dispersion effects) method [52]. Experimental data for H₂S are as follows; the H–S bond length is 1.33 Å and the H–S–H bond angle is 92.1° [53]. Accordingly, we have confirmed that WB97XD functional gives very close results to do experimental data and more accurate compared to B3LYP functional. Adsorption geometries were obtained by position the H₂S molecule close to the surface of all metal doped graphene structures and releasing it. Optimized geometries are shown in Fig. 3.

The obtained adsorption energies are listed in Table 2. According to the results, it is seen that all metal doped graphene structures can adsorb H₂S gas. The lowest ΔE was calculated as -71.0 kJ/mol. The fact that these values are not too low means that the amount of energy required for desorption is not too high. Considering the ΔH and ΔG values, all processes are exothermic and occur spontaneously. Compared

Table 2 Thermodynamic properties for H₂S adsorbed metal doped graphenes (values are in unit of kJ/mol)

Structure	ΔE	ΔH	ΔG
H ₂ S/Ti-graphene	-67.4	-69.9	-32.3
H ₂ S/V-graphene	-71.0	-73.5	-37.9
H ₂ S/Cr-graphene	-65.6	-68.1	-29.4
H ₂ S/Sc-graphene	-54.4	-56.9	-29.4

Table 3 Bond distances (d) between metal atoms and carbon atoms before and after H_2S adsorption (values are in unit \AA)

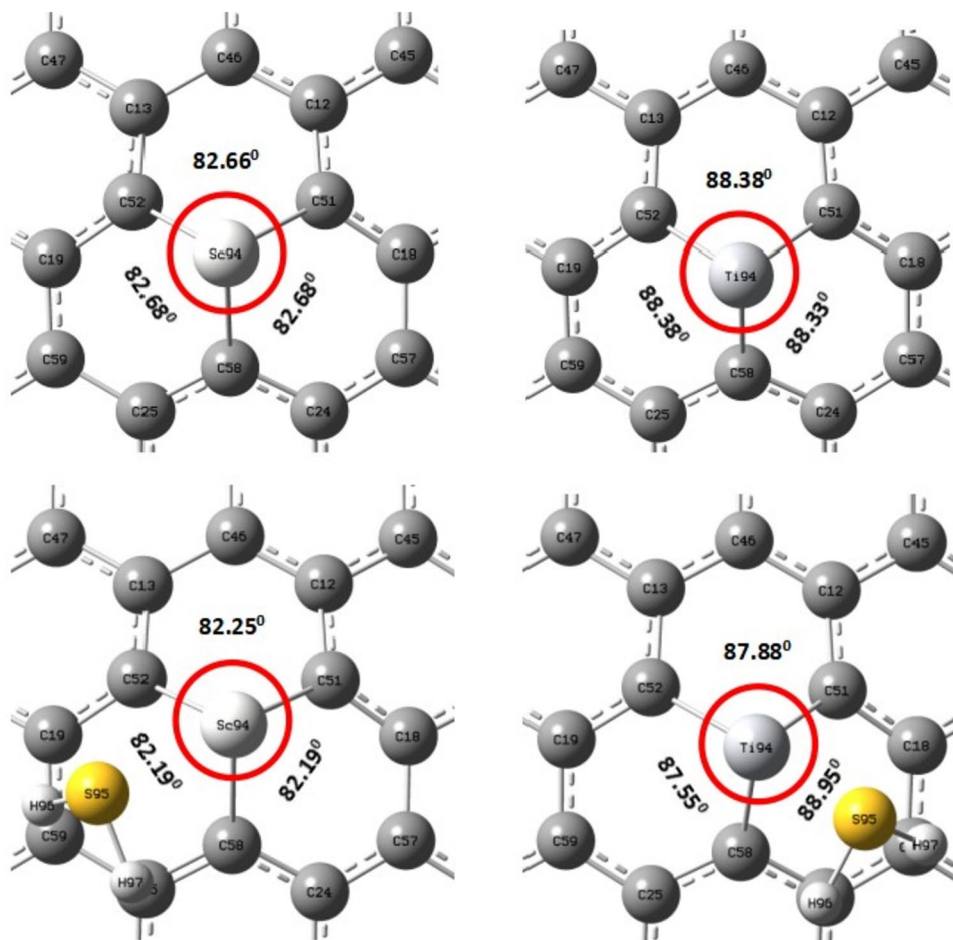
Structure	d_{M-C51}	d_{M-C52}	d_{M-C58}
Ti-graphene	1.916	1.916	1.917
H_2S /Ti-graphene	1.954	1.904	1.909
V-graphene	1.886	1.883	1.876
H_2S /V-graphene	1.866	1.880	1.890
Cr-graphene	1.874	1.874	1.875
H_2S /Cr-graphene	1.875	1.875	1.883
Sc-graphene	2.056	2.057	2.058
H_2S /Sc-graphene	2.060	2.082	2.065

to the adsorption energies of the pristine graphene structure, metal atoms both increased the H_2S adsorption ability and ensured spontaneous adsorption. The changes in bond distances between metal atoms and carbon atoms before and after H_2S adsorption were investigated. The calculated values are listed in Table 3. According to the values in the table, it can be said that all metal atoms are in a movement towards the H_2S molecule. In proportion to this, the bond distance with some of the carbon atoms increased. Figures 4 and 5 show the bond angles of metal doped graphene structures

before and after adsorption. The reason why the Sc-graphene structure has the lowest bond angle is that it is the structure with the highest C51-, C52- and C58-M bond length values in Table 3. Also, atom labels are shown in Figs. 4 and 5. These labels were used in both Tables 3 and 7.

In order to compare the H_2S adsorption on the materials used in this study with in the literature, the ΔE values of the H_2S molecule are listed in Table 4. According to these values, it is seen that the graphene structure is a better H_2S adsorbent material compared to other carbon structures such as CNT and fullerene. The very low energy of Fe and Pt doped graphene structures is undesirable in terms of desorption. In addition, considering the ΔE values of pristine graphene and Sc doped graphene, it is shown that Sc metal is not effective in adsorption.

The electronic characteristics of the structures were determined by analyzing the HOMO–LUMO gap energy (E_g) values with the difference between the calculated HOMO and LUMO energies. The HOMO, LUMO, E_g and ΔE_g values of the metal doped graphenes before and after adsorption are tabulated in Table 5. The E_g has been shown to be a good indicator for determining the sensitivity of nanosensors on numerous times [67]. There is also a relation between E_g and

Fig. 4 Illustration of atom labels and bond angles of Sc and Ti doped graphene structures before and after adsorption

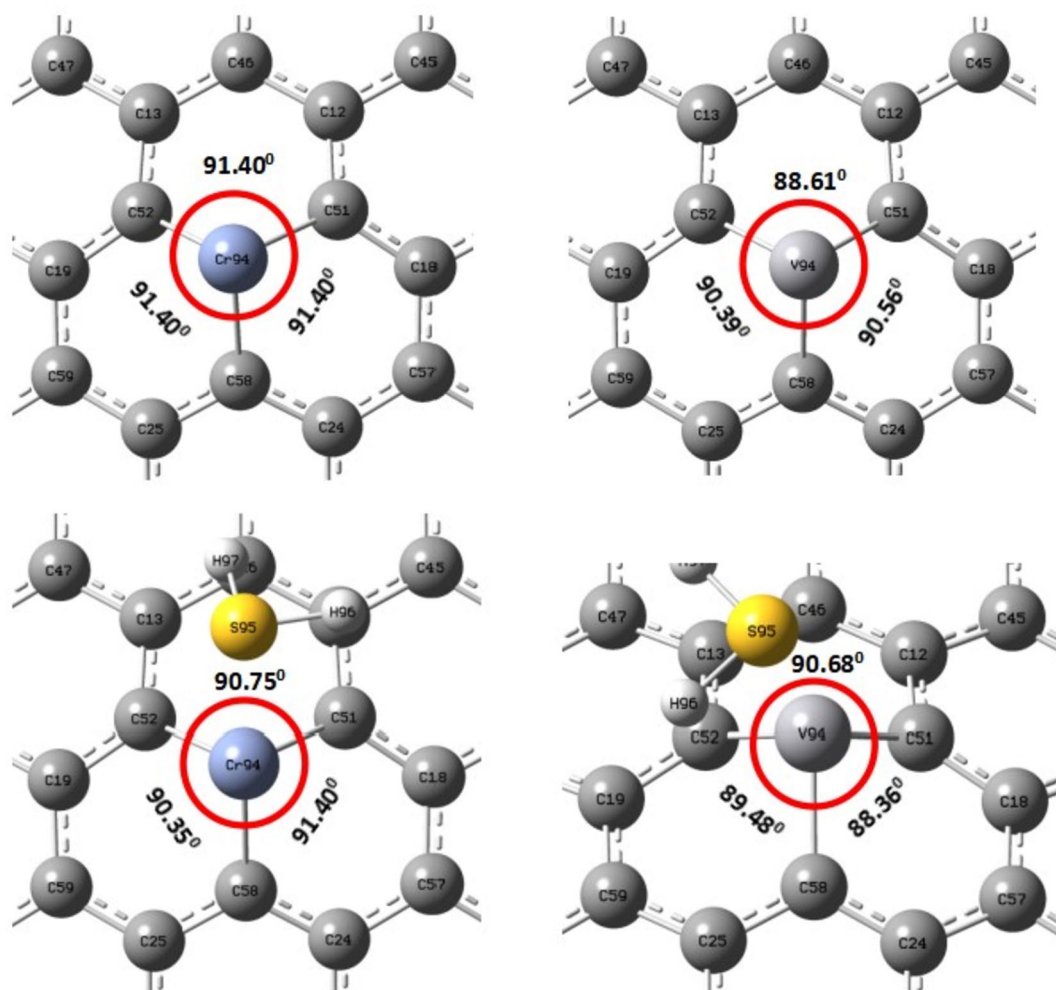


Fig. 5 Illustration of atom labels and bond angles of Cr and V doped graphene structures before and after adsorption

electrical conductivity (σ), which has also been mentioned in [68, 69]:

$$\sigma = AT^{3/2} \exp[-E_g/(2\kappa T)] \quad (6)$$

here κ is the Boltzmann's constant, A ($electrons/m^3 K^{3/2}$) is a constant and T is absolute temperature. There are a number of papers that verifies the use of this formula [70, 71]. Equation (6) indicates when E_g changes, the population of conduction electrons changes exponentially. As a result, the change in electrical conductivity indicates the presence of the chemical (H_2S for this study) in the environment. According to the results in Table 5, there is a significant change only for the Cr-graphene structure. A change of 24.8 kJ/mol was observed in the E_g of this structure. There was no significant change in other structures.

NBO population analysis was performed to analyze the atomic charge distributions in the interactions. In Table 6, the atomic charges of metal atoms in all structures and the total charge of the H_2S compound are given. When the NBO charges in the table are examined, electron transfer occurred from the H_2S molecule to the metal atom in all processes. Table 7 lists the energies calculated from the second-order perturbation theory analysis. This table lists the stabilization energy $E^{(2)}$ between electron donor orbital i , electron acceptor orbital j , and their interactions. The larger $E^{(2)}$, the stronger the interaction between them, and the greater the tendency for i to provide electrons to j , meaning the more charge will be transferred [72]. The stabilization energy $E^{(2)}$ associated with electron delocalization between donor and acceptor is calculated by the following equation [73].

Table 4 H₂S adsorption energy values of some materials in the literature

Structure	[Method]-[Basis set]	ΔE (kJ/mol)	Reference
B doped C ₆₀	[B3LYP] -[3-21G]	-32.3	[54]
Si doped C ₆₀	[B3LYP] -[3-21G]	-10.6	[54]
S doped C ₆₀	[B3LYP] -[3-21G]	-9.4	[54]
P doped C ₆₀	[B3LYP] -[3-21G]	-8.2	[54]
N doped C ₆₀	[B3LYP] -[3-21G]	27.7	[54]
Cu doped MoSe ₂	[GGA-PBE]	-126.9	[55]
Pt doped HAGNR	[GGA-PBE]—[LCAO]	-397.0	[56]
Pt doped NAGNR	[GGA-PBE]—[LCAO]	-375.5	[56]
Pt decorated graphene	[GGA-PBE]—[PAO]	-179.3	[57]
Fe doped graphene	[GGA-PBE]—[LCAO]	-98.6	[33]
N doped SiNR	[GGA-PBE]—[double zeta polarized]	-179.5	[58]
B doped SiNR	[GGA-PBE]—[double zeta polarized]	-86.8	[58]
N doped CNT	[GGA-PBE]—[DZDP]	76.0	[9]
Pristine CNT	[GGA-PBE]—[DZDP]	77.3	[9]
B doped CNT	[GGA-PBE]—[DZDP]	58.7	[9]
ZGNR	[GGA-PBE]—[unpolarized]	-24.3	[3]
S doped graphene	[GGA-PBE]—[DNP/6-31G(d,p)]	-40.5	[59]
Ni doped MoS ₂	[GGA-PBE]—[DNP]	-127.3	[60]
Au modified graphene	[GGA-PBE]	-86.8	[61]
Pristine graphene	[GGA-PBE]	-59.5	[61]
α -Fe ₂ O ₃ (001)	[GGA-PBE]	-64.6	[62]
Mg doped graphene	[GGA-PBE]—[DNP]	-45.3	[63]
B doped CNT	[B3LYP]—[6-31G(d,p)/LANL2DZ]	-67.4	[64]
Ga doped CNT	[B3LYP]—[6-31G(d,p)/LANL2DZ]	-108.7	[64]
Ge doped CNT	[B3LYP]—[6-31G(d,p)/LANL2DZ]	-48.5	[64]
Pristine graphene	[GGA-PW91]	-34.7	[65]
Ni doped graphene	[GGA-PW91]	-93.6	[65]
Cu doped graphene	[GGA-PW91]	-110.9	[65]
Zn doped graphene	[GGA-PW91]	-111.9	[65]
Fe-ZSM-12	[B3LYP]—[6-31G(d,p)/LANL2DZ]	-78.0	[66]
Co-ZSM-12	[B3LYP]—[6-31G(d,p)/LANL2DZ]	-76.0	[66]
Ni-ZSM-12	[B3LYP]—[6-31G(d,p)/LANL2DZ]	-92.0	[66]
Cu-ZSM-12	[B3LYP]—[6-31G(d,p)/LANL2DZ]	-55.0	[66]
Zn-ZSM-12	[B3LYP]—[6-31G(d,p)/LANL2DZ]	-76.0	[66]
Ti doped graphene	[WB97XD]—[6-31G(d,p)/LANL2DZ]	-67.4	[This study]
V doped graphene	[WB97XD]—[6-31G(d,p)/LANL2DZ]	-71.0	[This study]
Cr doped graphene	[WB97XD]—[6-31G(d,p)/LANL2DZ]	-65.6	[This study]
Sc doped graphene	[WB97XD]—[6-31G(d,p)/LANL2DZ]	-54.4	[This study]

PAO Pseudo Atomic Orbitals, LCAO Linear Combination of Atomic Orbitals, DZDP Double Zeta Double Polarized, DNP Double Numerical Plus Polarization

$$E^{(2)} = q_i \frac{F_{ij}^2}{E_i - E_j} \quad (7)$$

For each donor NBO (i) and acceptor NBO (j), where q_i is the orbital occupancy, $E_i - E_j$ are the diagonal elements, and F_{ij} is the off-diagonal NBO fock matrix element. $E^{(2)}$

values between Lewis type (donor) NBOs and non-Lewis (acceptor) type NBOs show that the electron density is significantly delocalized from carbon atoms to metal atoms. Here there are molecular LP-LP* and BD-LP* interactions. The LP-LP* transition exhibited higher stabilization energy. Moreover, BD-LP* stands out as an important transition,

Table 5 Electronic characteristics of metal-doped graphene structures including HOMO and LUMO energies and HOMO–LUMO gap energy changes for before and after H₂S adsorption (values are in unit *kJ/mol*)

Structure		E _{HOMO}	E _{LUMO}	E _g	ΔE _g
Ti-graphene	αMOs	-513.8	-79.9	433.9	
	βMOs	-599.4	-164.5	434.9	
H ₂ S/Ti-graphene	αMOs	-511.1	-77.9	433.2	-0.8
	βMOs	-592.5	-162.2	430.3	-4.6
V-graphene	αMOs	-526.1	-82.2	443.9	
	βMOs	-605.4	-157.2	448.2	
H ₂ S/V-graphene	αMOs	-518.0	-76.8	441.2	-2.8
	βMOs	-597.0	-154.2	442.8	-5.4
Cr-graphene	αMOs	-536.4	-130.5	405.8	
	βMOs	-608.1	-151.0	457.1	
H ₂ S/Cr-graphene	αMOs	-532.8	-102.2	430.6	24.8
	βMOs	-601.5	-149.2	452.3	-4.8
Sc-graphene		-522.5	-192.8	329.7	
H ₂ S/Sc-graphene		-521.4	-191.1	330.3	0.5

although it exhibits lower stability. In Table 6, the most positive charge among the metal atoms belongs to the Sc atom. This means that Sc–C bonds are more ionic than other metal–C bonds. Therefore, the energy difference between the acceptor Sc atom and the donor C atoms is larger than the energy difference between the other metal atoms and the donor C atoms.

Chemical hardness (η), chemical potential (μ) and electronegativity (χ) were calculated for metal doped graphenes and tabulated in Table 8. Detailed information on the calculation of these parameters is given in Supplementary Material. There was no significant change in chemical hardness, chemical potential and electronegativity of Ti, V and Sc doped graphene structures after H₂S adsorption. In other words, the stability and chemical reactivity of the structures

Table 6 NBO charges of metal atoms and H₂S molecule before and after H₂S adsorption of metal-doped graphene structures (values are in unit *e*)

Structure	Metal atomic charge	H ₂ S total charge
Ti-graphene	+1.107	-
H ₂ S/Ti-graphene	+0.855	+0.246
V-graphene	+0.766	-
H ₂ S/V-graphene	+0.431	+0.265
Cr-graphene	+0.655	-
H ₂ S/Cr-graphene	+0.413	+0.218
Sc-graphene	+1.482	-
H ₂ S/Sc-graphene	+1.347	+0.168

Table 7 A part of calculated second order perturbation stabilization energy (E⁽²⁾) for donor–acceptor NBO interaction for metal-doped graphene structures

Donor NBO (i)	Acceptor NBO (j)	E ⁽²⁾ (<i>kcal/mol</i>)
LP(1)C(51)	LP*(3)Sc(94)	78.40
LP(1)C(52)	LP*(1)Sc(94)	136.05
LP(1)C(58)	LP*(2)Sc(94)	129.48
BD(2)C(12)–C(51)	LP*(1)V(94)	14.93
BD(2)C(19)–C(52)	LP*(1)V(94)	14.79
BD(2)C(24)–C(58)	LP*(1)V(94)	16.12
BD(2)C(18)–C(51)	LP*(1)Ti(94)	18.46
BD(2)C(13)–C(52)	LP*(1)Ti(94)	18.53
BD(2)C(25)–C(58)	LP*(1)Ti(94)	18.35
BD(2)C(12)–C(51)	LP*(1)Cr(94)	9.88
BD(2)C(13)–C(52)	LP*(1)Cr(94)	9.91
BD(2)C(24)–C(58)	LP*(1)Cr(94)	9.84

LP(1) and BD(2) denote 1st lone pair and 2-center bond for bonding NBOs, respectively. LP*(1), LP*(2) and LP*(3) denote 1st, 2nd and 3rd lone pair for anti-bonding NBOs, respectively

is preserved. However, the chemical hardness of the Cr-graphene structure (especially for αMOs) increased and the structure became harder.

Figure 6 shows the HOMO and LUMO illustrations of Cr doped graphene and H₂S molecule adsorbed Cr doped graphenes. When the HOMO LUMO analysis is examined, HOMOs are spread on the graphene sheet, while LUMOs are located around the metal atom. The most obvious result here is the reduction of LUMOs around the metal atom after adsorption, especially in

Table 8 The η , μ and χ values of metal-doped graphene structures before and after H₂S adsorption (values are in unit *kJ/mol*)

Structure		η	μ	χ
Ti-graphene	αMOs	217.0	-296.8	296.8
	βMOs	217.4	-381.9	381.9
H ₂ S/Ti-graphene	αMOs	216.6	-294.5	294.5
	βMOs	215.1	-377.3	377.3
V-graphene	αMOs	222.0	-304.1	304.1
	βMOs	224.1	-381.3	381.3
H ₂ S/V-graphene	αMOs	220.6	-297.4	297.4
	βMOs	221.4	-375.6	375.6
Cr-graphene	αMOs	203.0	-333.5	333.5
	βMOs	228.6	-379.5	379.5
H ₂ S/Cr-graphene	αMOs	215.3	-317.5	317.5
	βMOs	226.1	-375.4	375.4
Sc-graphene		165.0	-357.7	357.7
H ₂ S/Sc-graphene		165.2	-356.2	356.2

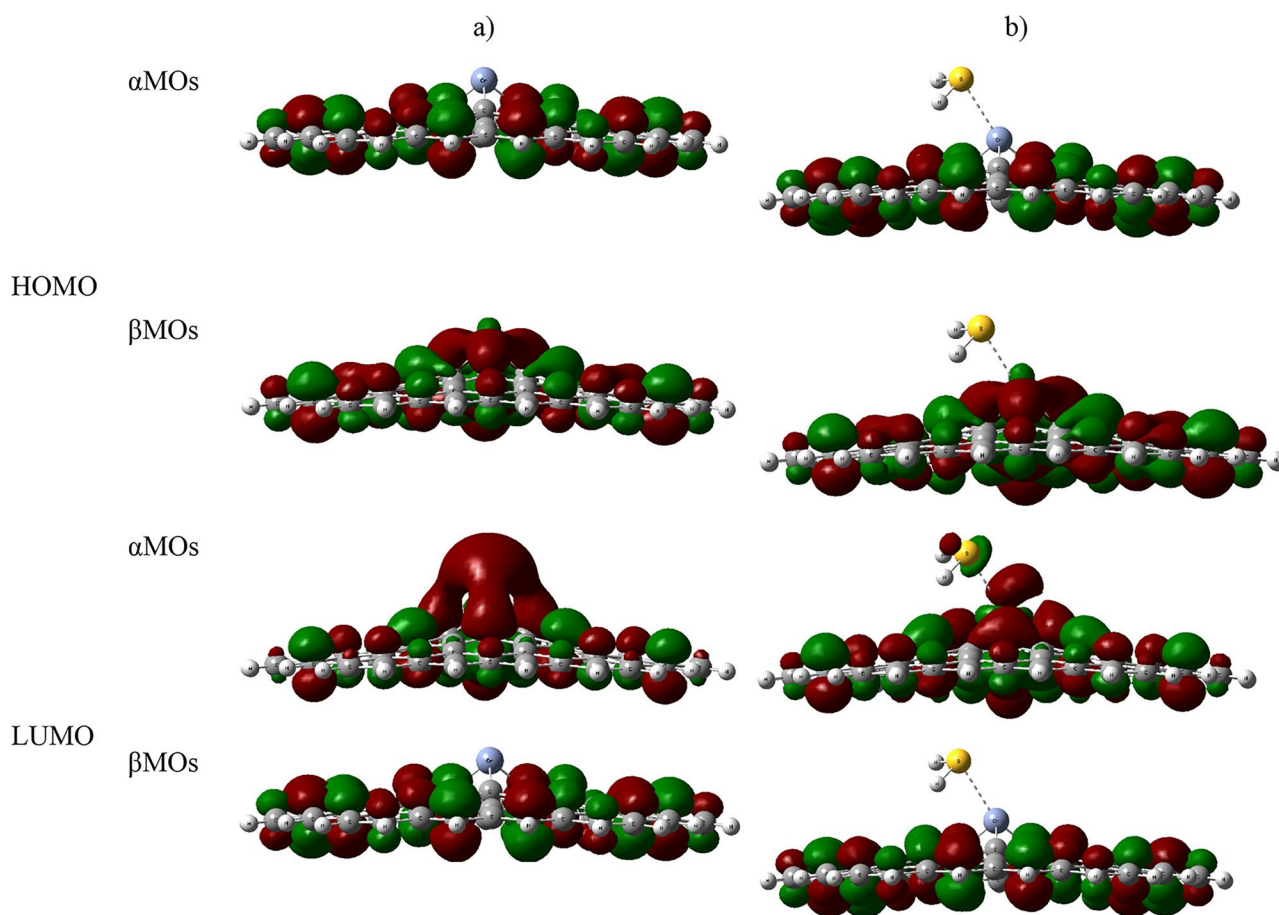


Fig. 6 Illustrations of HOMO and LUMO distributions of **a** Cr-graphene structure and **b** H₂S/Cr-graphene system

a molecular orbitals. This refers to the increase in the total charge of the H₂S molecule, that is, it donates electrons. HOMO–LUMO representations of other structures are presented in Figs. 7, 8 and 9. Accordingly, for the Ti doped graphene structure, β MOs HOMOs and α MOS LUMOs are located around the metal atom. Only for α MOs LUMOs, orbital displacements occurred before and after adsorption. For the V doped graphene structure, a decrease in α MOs LUMOs occurred after adsorption. According to the HOMO and LUMO analysis for the Sc doped graphene structure, there is an increase in the HOMOs around the metal after adsorption.

The TDOS and PDOS of Cr doped graphene and H₂S adsorbed Cr doped graphene have been presented in Fig. 10. As can be seen the Fig. 10, we see that the HOMO–LUMO gap increases in α MOs. Thus, it can be concluded that there is a change in electrical conductivity. It is seen in Figs. S1–S3 that the TDOS and PDOS plots of other structures do not change significantly. Moreover,

the electrostatic potential (ESP) distributions for Cr doped graphene before and after H₂S adsorption have been shown in Fig. 11. Blue and red colors were respectively defined on the ESP maps by the Van der Waals surface's positive and negative areas [74, 75]. In Fig. 11, blue colors are seen in the metal atom before adsorption, but the blue colors decrease after adsorption. In this case, we can say that the positively charged H₂S molecule is adsorbed in blue and the blue colors are reduced due to the electron gain from the metal atom. ESP maps of other structures are presented in Figs. S4–S6.

Johnson et al. group [76] has proposed the RDG analysis, which enables determining the kind of interactions that take place between two species. By examining the reduced gradient of the density as a function of the electron density multiplied by the sign of the second eigenvalue of the Hessian matrix, this analysis has been utilized to look at the many non-covalent interactions that are still present in the molecules. The greatest eigenvalue is known to be λ_2 in

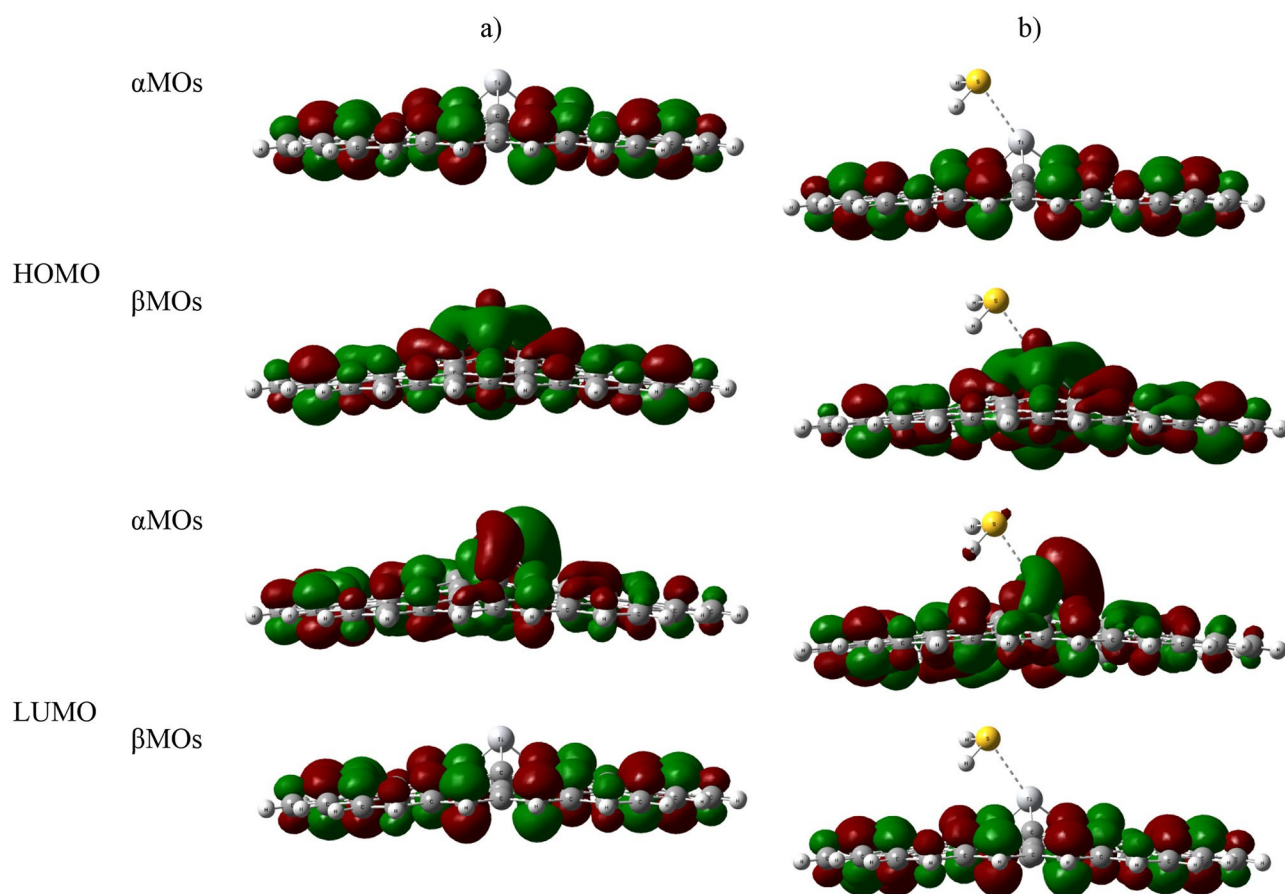


Fig. 7 Illustrations of HOMO and LUMO distributions of **a** Ti-graphene structure and **b** H₂S/Ti-graphene system

Hessian matrix. Based on this, one could create a distinction between the dissimilar kinds of noncovalent interactions. Figure 12 presents RDG scatter map and isosurface map for H₂S/V-graphene system (since it is the system with the lowest adsorption energy). RDG maps of other structures are presented in Figs. S7–S9.

According to the RDG analysis, for metal doped graphenes, the Van der Waals interactions are indicated by values near zero. All scatter maps and isosurface maps of RDG show us that the interactions are typically VdW-type interactions for H₂S adsorbed metal doped graphenes. It is important to note that extremely strong interactions do not detect molecules since they show that the adsorbate is difficult to desorb and that the system requires more time to recover. The traditional transition theory forecasts a significantly longer recovery time in the event that the energy

of adsorption rises significantly equation is employed to elucidate this situation:

$$\tau = (\nu_0)^{-1} \exp(-\Delta E/kT) \quad (8)$$

Here τ is the recovery time, ΔE is adsorption energy, T is adsorption temperature (298.15 K), k is the Boltzmann constant ($\sim 8.368 \times 10^{-3}$ kJ/mol) and the ν_0 is attempt frequency ($\sim 10^{12}$ s⁻¹) [77]. According to this equation, the greater the ΔE value, resulting in progressively longer recovery times. In other words, the material adsorbed to the surface takes longer to separate from the surface. The recovery time of the Cr-graphene structure, which has an electronic sensor feature, is 0.26 s. The surface recovery times of Ti-, V- and Sc-graphene structures were calculated as 0.54, 2.28 and 0.003 s, respectively.

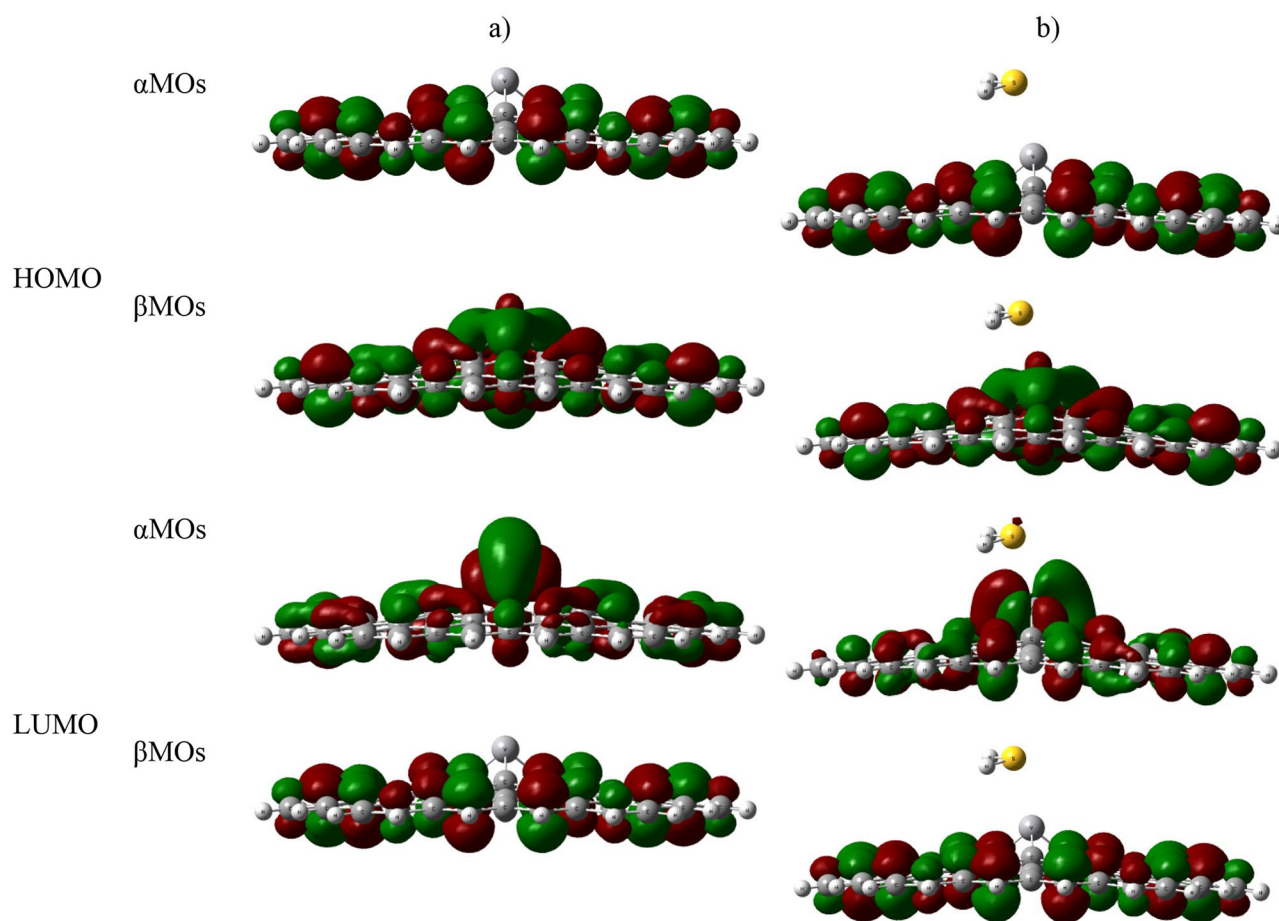
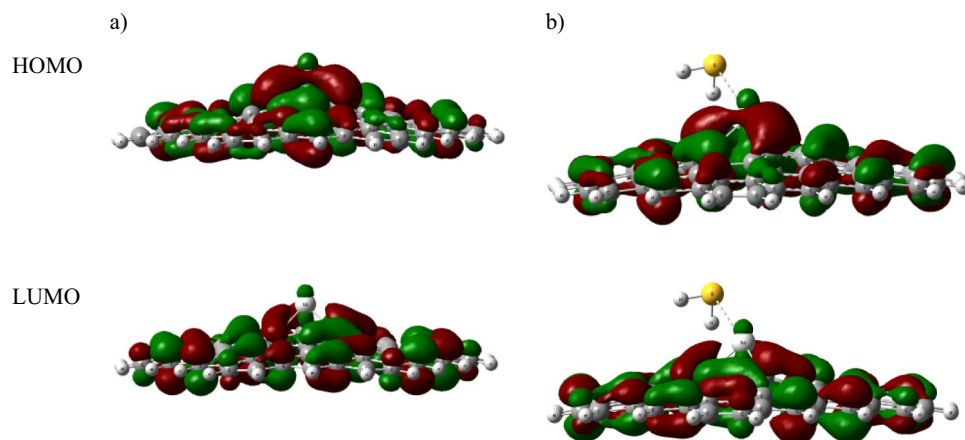


Fig. 8 Illustrations of HOMO and LUMO distributions of **a** V-graphene structure and **b** H₂S/V-graphene system

Fig. 9 Illustrations of HOMO and LUMO distributions of **a** Sc-graphene structure and **b** H₂S/Sc-graphene system



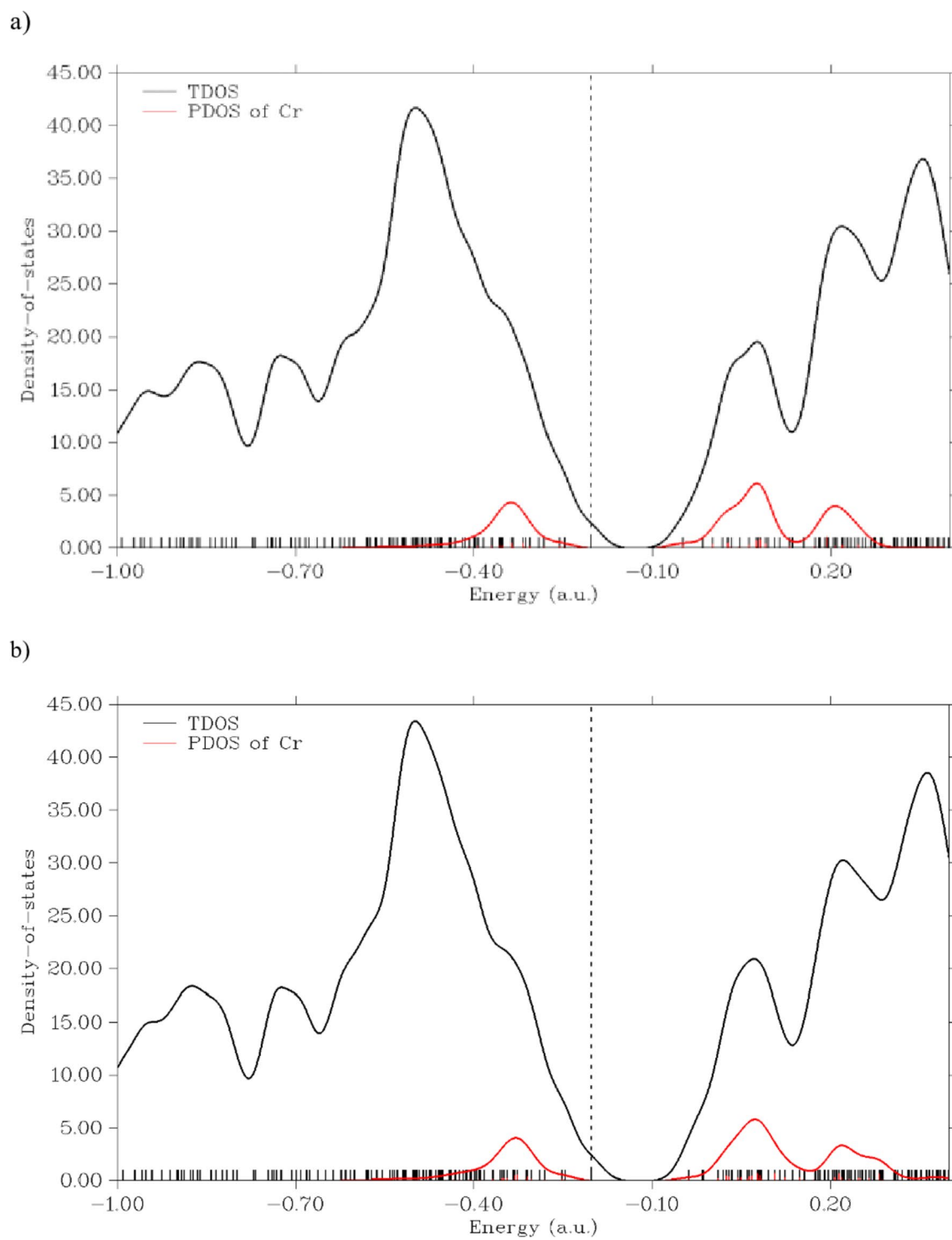
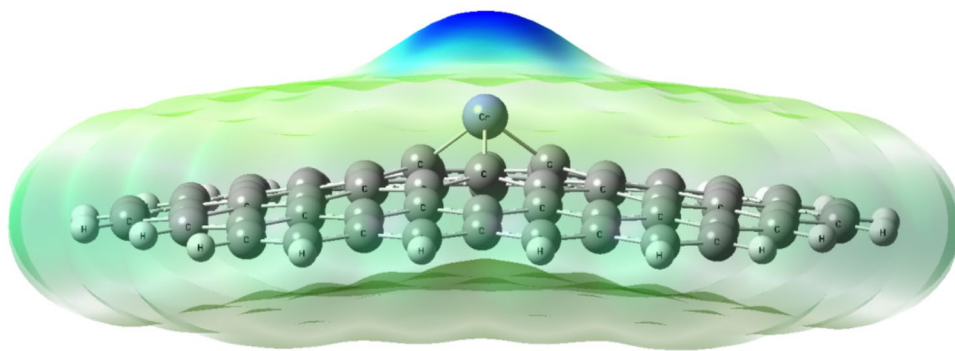


Fig. 10 TDOS and PDOS plots of **a** Cr-graphene and **b** H₂S/Cr-graphene

Fig. 11 ESP distribution maps of **a** Cr-graphene and **b** H₂S/Cr-graphene

a)



b)

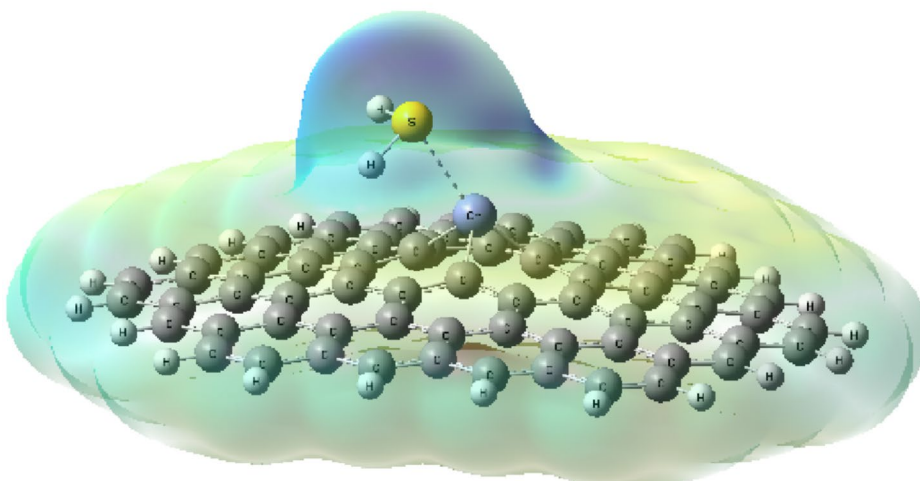
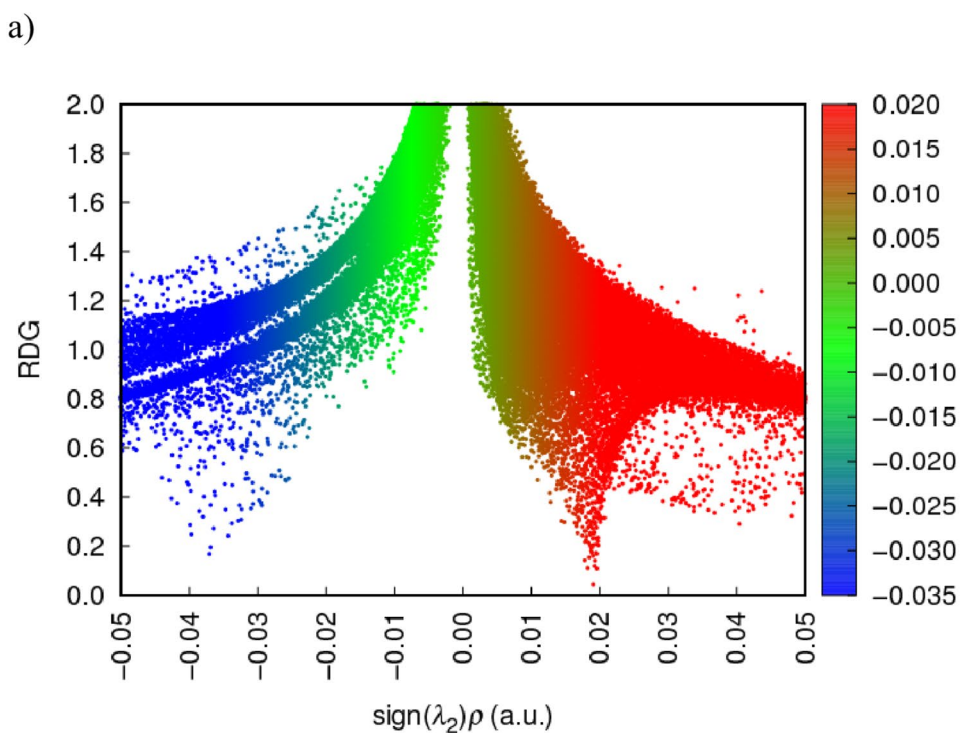
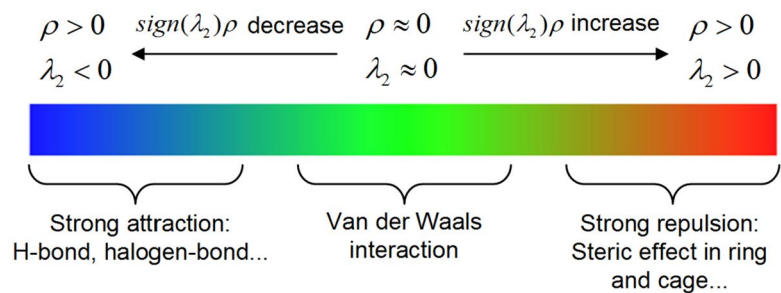
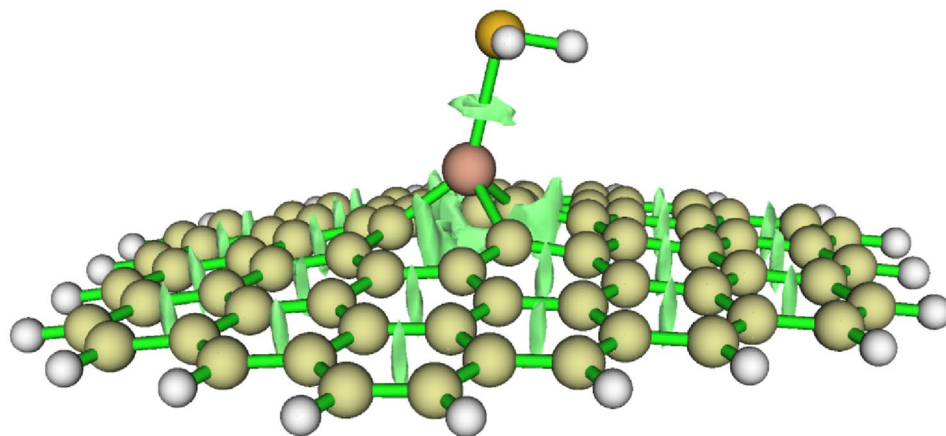


Fig. 12 **a** RDG scatter map and **b** RDG isosurface map of H_2S/V -graphene system



b)



Conclusions

In this study, Ti, V, Cr and Sc doped graphene nanosheets, along with the molecular system formed by hydrogen sulfide, were investigated for their adsorption and sensor properties using the DFT method. As a result of the thermodynamic data, it was revealed that all metal-doped graphene structures adsorbed the H₂S molecule spontaneously. Compared to the literature, the ΔE values are not found to be enough to make desorption difficult. In the light of RDG analyses, all interactions were realized as Van der Waals interactions. In addition, in all interactions, there is charge transfer between the H₂S molecule and metal atoms. The HOMO–LUMO gap change of the Cr doped graphene structure before and after adsorption was calculated as 24.8 kJ/mol. For other structures, this change remained insignificant. Consequently, this finding confirms that the structure in question could be used as an electronic sensor material for the H₂S molecule.

Supplementary Information The online version contains supplementary material available at <https://doi.org/10.1007/s11224-023-02265-2>.

Acknowledgements The numerical calculations reported in this paper were partially performed at TUBITAK ULAKBIM, High Performance and Grid Computing Center (TRUBA resources).

Author contributions All authors contributed to the study conception and design. Methodology, Software, Writing—Original Draft were performed by [Ömer Faruk TUNALI] and [Numan YUKSEL]. Validation, Formal analysis, Writing—Review & Editing, Supervision were performed by [Gökhan GECE]. Conceptualization, Validation, Formal analysis, Writing—Review & Editing, Supervision were performed by [Mehmet Ferdi FELLAH]. All authors read and approved the final manuscript.

Funding The authors declare that no funds, grants, or other support were received during the preparation of this manuscript.

Data availability There is no data availability.

Declarations

Competing interests The authors declare no competing interests.

References

- Zeng H, Wang L, Zhang D, Yan P, Nie J, Sharma VK, Wang C (2019) Highly efficient and selective removal of mercury ions using hyperbranched polyethylenimine functionalized carboxymethyl chitosan composite adsorbent. *Chem Eng J*. <https://doi.org/10.1016/j.cej.2018.10.001>
- Wang S, Nam H, Lee D, Nam H (2022) H₂S gas adsorption study using copper impregnated on KOH activated carbon from coffee residue for indoor air purification. *J Environ Chem Eng*. <https://doi.org/10.1016/j.jece.2022.108797>
- Salih E, Ayesh AI (2020) DFT investigation of H₂S adsorption on graphenenanosheets and nanoribbons: Comparative study. *Superlattices Microstruct*. <https://doi.org/10.1016/j.spmi.2020.106650>
- Ozekmekci M, Salkic G, Fellah MF (2015) Use of zeolites for the removal of H₂S: A mini-review. *Fuel Process Technol*. <https://doi.org/10.1016/j.fuproc.2015.08.015>
- Agbroko OW, Piler K, Benson TJ (2017) A comprehensive review of H₂S scavenger technologies from oil and gas streams. *ChemBioEng Rev*. <https://doi.org/10.1002/cben.201600026>
- Nam H, Wang S, Jeong HR (2018) TMA and H₂S gas removals using metal loaded on rice husk activated carbon for indoor air purification. *Fuel*. <https://doi.org/10.1016/j.fuel.2017.10.089>
- Shah MS, Tsapatsis M, Siepmann JI (2017) Hydrogen sulfide capture: From absorption in polar liquids to oxide, zeolite, and metal-organic framework adsorbents and membranes. *Chem Rev*. <https://doi.org/10.1021/acs.chemrev.7b00095>
- Habeeb O, Ramesh K, Ali GA, Yunus R, Thanusha T, Olalere O (2016) Modeling and optimization for H₂S adsorption from wastewater using coconut shell based activated carbon. *Aust J Basic Appl Sci* 10:136–147
- Srivastava R, Suman H, Shrivastava S, Srivastava A (2019) DFT Analysis of Pristine and functionalized Zigzag CNT: A case of H₂S sensing. *Chem Phys Lett*. <https://doi.org/10.1016/j.cplett.2019.07.003>
- El-Sherbiny I, Salih E (2018) In: Kanchi S, Ahmed S (ed) Green synthesis of metallic nanoparticles using biopolymers and plant extracts: Synthesis, characterization and their applications. Wiley, New York. <https://doi.org/10.1002/9781119418900.ch10>
- Dresselhaus M, Terrones M (2013) Carbon-based nanomaterials from a historical perspective. *Proc IEEE*. <https://doi.org/10.1109/JPROC.2013.2261271>
- Iijima S, Ichihashi T (1993) Single-shell carbon nanotubes of 1-nm diameter. *Nature*. <https://doi.org/10.1038/363603a0>
- Baptista F, Belhout S, Giordani S, Quinn S (2015) Recent developments in carbon nanomaterial sensors. *Chem Soc Rev*. <https://doi.org/10.1039/C4CS00379A>
- Lan G, Tang L, Dong J, Nong J, Luo P, Li X, Li Z, Zhang Y, Dai Y, Wang W, Shi H, Wei W (2023) Enhanced asymmetric light-plasmon coupling in graphene nanoribbons for high-efficiency transmissive infrared modulation. *Laser Photonics Rev*. <https://doi.org/10.1002/lpor.202300469>
- Tang T, Zhou M, Lv J, Cheng H, Wang H, Qin D, Hu G, Liu X (2022) Sensitive and selective electrochemical determination of uric acid in urine based on ultrasmall iron oxide nanoparticles decorated urchin-like nitrogen-doped carbon. *Colloids Surf B*. <https://doi.org/10.1016/j.colsurfb.2022.112538>
- Mubeen S, Zhang T, Chartuprayoon N, Rheem Y, Mulchandani A, Myung NV, Deshusses MA (2010) Sensitive detection of H₂S using gold nanoparticle decorated single-walled carbon nanotubes. *Anal Chem*. <https://doi.org/10.1021/ac901871d>
- Tsai JH, Jeng FT, Chiang HL (2001) Removal of H₂S from exhaust gas by use of alkaline activated carbon. *Adsorption*. <https://doi.org/10.1023/A:1013142405297>
- Bandosz TJ (2002) On the adsorption/oxidation of hydrogen sulfide on activated carbons at ambient temperatures. *J Colloid Interface Sci*. <https://doi.org/10.1006/jcis.2001.7952>
- Yan R, Liang DT, Tsen L, Tay JH (2002) Kinetics and mechanisms of H₂S adsorption by alkaline activated carbon. *Environ Sci Technol*. <https://doi.org/10.1021/es0205840>
- Kaliva AN, Smith JW (1983) Oxidation of low concentrations of hydrogen sulfide by air on a fixed activated carbon bed. *Can J Chem Eng*. <https://doi.org/10.1002/cjce.5450610210>
- Águila JEC, Cocolletti HH, Cocolletti GH (2013) A theoretical analysis of the role of defects in the adsorption of hydrogen sulfide on graphene. *AIP Adv*. <https://doi.org/10.1063/1.4794953>
- Wang S, Sun H, Ang HM, Tadé MO (2013) Adsorptive remediation of environmental pollutants using novel graphene-based nanomaterials. *Chem Eng J*. <https://doi.org/10.1016/j.cej.2013.04.070>

23. Ou L, Song B, Liang H, Liu J, Feng X, Deng B, Sun T, Shao L (2016) Toxicity of graphene-family nanoparticles: a general review of the origins and mechanisms. *Part Fibre Toxicol*. <https://doi.org/10.1186/s12989-016-0168-y>
24. Geim AK, Novoselov KS (2007) The rise of graphene. *Nat Mater*. <https://doi.org/10.1038/nmat1849>
25. Dutta S, Manna A, Pati S (2009) Intrinsic half-metallicity in modified graphene nanoribbons. *Phys Rev Lett*. <https://doi.org/10.1103/PhysRevLett.102.096601>
26. Ren H, Li Q, Luo Y, Yang J (2009) Graphene nanoribbon as a negative differential resistance device. *Appl Phys Lett* doi 10(1063/1):3126451
27. Hernandez Y, Nicolosi V, Lotya M, Blighe FM, Sun Z, De S, McGovern IT, Holland B, Byrne M, Gun'Ko YK, Boland JJ, Niraj P, Duesberg G, Krishnamurthy S, Goodhue R, Hutchison J, Scardaci V, Ferrari AC, Coleman JN (2008) High-yield production of graphene by liquid-phase exfoliation of graphite. *Nat Nanotechnol*. <https://doi.org/10.1038/nnano.2008.215>
28. Li X, Zhang G, Bai X, Sun X, Wang X, Wang E, Dai H (2008) Highly conducting graphene sheets and Langmuir-Blodgett films. *Nat Nanotechnol*. <https://doi.org/10.1038/nnano.2008.210>
29. Tang Y, Yang Z, Dai X, Ma D, Fu Z (2013) Formation, stabilities, and electronic and catalytic performance of platinum catalyst supported on non-metal-doped graphene. *J Phys Chem C*. <https://doi.org/10.1021/jp400202e>
30. Ganji M, Sharifi N, Ahangari M (2014) Adsorption of H₂S molecules on non-carbonic and decorated carbonic graphenes: A van der Waals density functional study. *Comput Mater Sci*. <https://doi.org/10.1016/j.commatsci.2014.05.035>
31. Zhang YH, Han LF, Xiao YH, Jia DZ, Guo ZH, Li F (2013) Understanding dopant and defect effect on H₂S sensing performances of graphene: A first-principles study. *Comput Mater Sci*. <https://doi.org/10.1016/j.commatsci.2012.11.048>
32. Ganji MD, Sharifi N, Ardjmand M, Ahangari MG (2012) Pt-decorated graphene as superior media for H₂S adsorption: a first-principles study. *App Surf Sci*. <https://doi.org/10.1016/j.apsusc.2012.08.083>
33. Zhang HP, Luo XG, Song HT, Lin XY, Lu X, Tang Y (2014) DFT study of adsorption and dissociation behavior of H₂S on Fe-doped graphene. *App Surf Sci*. <https://doi.org/10.1016/j.apsusc.2014.08.141>
34. Borisova D, Antonov V, Proykova A (2013) Hydrogen sulfide adsorption on a defective graphene. *Int J Quantum Chem*. <https://doi.org/10.1002/qua.24077>
35. Hegde VI, Shirodkar SN, Tit N, Waghmare UV, Yamani ZH (2014) First principles analysis of graphene and its ability to maintain long-ranged interaction with H₂S. *Surf Sci*. <https://doi.org/10.1016/j.susc.2013.11.015>
36. Mohammadi-Manesh E, Vaezzadeh M, Saeidi M (2015) Cu- and CuO-decorated graphene as a nanosensor for H₂S detection at room temperature. *Surf Sci*. <https://doi.org/10.1016/j.susc.2015.02.002>
37. Gao X, Zhou Q, Wang J, Xu L, Zeng W (2020) Performance of intrinsic and modified graphene for the adsorption of H₂S and CH₄: a DFT study. *Nanomaterials*. <https://doi.org/10.3390/nano10020299>
38. Salmankhani A, Karami Z, Mashhadzadeh AH, Ganjali MR, Vatanpour V, Esmaeili A, Habibzadeh S, Saeb MR, Fierro V, Celzard A (2020) New insights into H₂S adsorption on graphene and graphene-like structures: a comparative DFT study. *C*. <https://doi.org/10.3390/c6040074>
39. Bayatsarmadi B, Zheng Y, Vasileff A, Qiao SZ (2017) Recent advances in atomic metal doping of carbon-based nanomaterials for energy conversion. *Small*. <https://doi.org/10.1002/smll.201700191>
40. Qiu HJ, Ito Y, Cong W, Tan Y, Liu P, Hirata A, Fujita T, Tang Z, Chen M (2015) Nanoporous graphene with single-atom nickel dopants: an efficient and stable catalyst for electrochemical hydrogen production. *Angew Chem Int Ed Engl*. <https://doi.org/10.1002/anie.201507381>
41. Sun H, Yang L, Wu H, Zhao L (2023) Effects of element doping on the structure and properties of diamond-like carbon films: a review. *Lubricants*. <https://doi.org/10.3390/lubricants11040186>
42. Frisch M, Trucks G, Schlegel H, Scuseria G, Robb M, Cheeseman J, Scalmani G, Barone V, Mennucci B, Petersson G (2015) Gaussian 09, Revision D. 01; Gaussian, Inc: Wallingford, CT
43. Kohn W, Sham LJ (1965) Self-consistent equations including exchange and correlation effects. *Phys Rev*. <https://doi.org/10.1103/PhysRev.140.A1133>
44. Chai JD, Head-Gordon M (2008) Systematic optimization of long-range corrected hybrid density functionals. *J Chem Phys* doi 10(1063/1):2834918
45. Tsuneda T, Hirao K (2014) Long-range correction for density functional theory. *Wiley Interdiscip Rev: Comput Mol Sci*. <https://doi.org/10.1002/wcms.1178>
46. Natan A, Kronik L, Shapira Y (2006) Computing surface dipoles and potentials of self-assembled monolayers from first principles. *App Surf Sci*. <https://doi.org/10.1016/j.apsusc.2006.03.052>
47. Kumar S, Sharma S, Karmaker R, Sinha D (2021) DFT study on the structural, optical and electronic properties of platinum group doped graphene. *Mater Today Commun*. <https://doi.org/10.1016/j.mtcomm.2020.101755>
48. Wong MW (1996) Vibrational frequency prediction using density functional theory. *Chem Phys Lett*. [https://doi.org/10.1016/0009-2614\(96\)00483-6](https://doi.org/10.1016/0009-2614(96)00483-6)
49. Lu T, Chen F (2012) Multiwfn: A multifunctional wavefunction analyzer. *J Comput Chem*. <https://doi.org/10.1002/jcc.22885>
50. Kumar N, Sharma M, Sharma JD, Ahluwalia PK (2015) Study of magnetism in nano structures of graphene and functionalized graphene: a first principle study. *Indian J Phys*. <https://doi.org/10.1007/s12648-014-0526-2>
51. Nagarajan V, Nivedhana R, Chandiramouli R (2023) Nucleobases adsorption studies on chair graphene nanosheets – A DFT outlook. *Inorg Chem Commun*. <https://doi.org/10.1016/j.inoche.2023.110683>
52. Bokhimi X (2019) Atomic and electronic properties of a 155 H₂S cluster under pressure. *ACS Omega*. <https://doi.org/10.1021/acsomega.9b00705>
53. Cook RL, De Lucia FC, Helminger P (1975) Molecular force field and structure of hydrogen sulfide: recent microwave results. *J Mol Struct*. [https://doi.org/10.1016/0022-2860\(75\)80094-9](https://doi.org/10.1016/0022-2860(75)80094-9)
54. Yousefian Z, Ghasemy E, Askarieh M, Rashidi A (2019) Theoretical studies on B, N, P, S, and Si doped fullerenes toward H₂S sensing and adsorption. *Phys E*. <https://doi.org/10.1016/j.physe.2019.113626>
55. Ayesh AI (2022) H₂S and SO₂ adsorption on Cu doped MoSe₂: DFT investigation. *Phys Lett A*. <https://doi.org/10.1016/j.physleta.2021.127798>
56. Salih E, Ayesh AI (2021) Computational study of metal doped graphene nanoribbon as a potential platform for detection of H₂S. *Mater Today Commun*. <https://doi.org/10.1016/j.mtcomm.2020.101823>
57. Bo Z, Guo X, Wei X, Yang H, Yan J, Cen K (2019) Density functional theory calculations of NO₂ and H₂S adsorption on the group 10 transition metal (Ni, Pd and Pt) decorated graphene. *Phys E*. <https://doi.org/10.1016/j.physe.2019.01.012>
58. Aghaei SM, Monshi MM, Calizo I (2016) A theoretical study of gas adsorption on silicene nanoribbons and its application in a highly sensitive molecule sensor. *RSC Adv*. <https://doi.org/10.1039/C6RA21293J>
59. Faye O, Raj A, Mittal V, Beye AC (2016) H₂S adsorption on graphene in the presence of sulfur: A density functional theory study. *Comput Mater Sci*. <https://doi.org/10.1016/j.commatsci.2016.01.034>
60. Wei H, Gui Y, Kang J, Wang W, Tang C (2018) A DFT study on the adsorption of H₂S and SO₂ on Ni doped MoS₂ monolayer. *Nanomaterials*. <https://doi.org/10.3390/nano8090646>

61. Zhang X, Yu L, Wu X, Hu W (2015) Experimental sensing and density functional theory study of H₂S and SOF₂ adsorption on Au-modified graphene. *Adv Sci*. <https://doi.org/10.1002/advs.201500101>
62. Lin C, Qin W, Dong C (2016) H₂S adsorption and decomposition on the gradually reduced α -Fe₂O₃(001) surface: A DFT study. *App Surf Sci*. <https://doi.org/10.1016/j.apsusc.2016.06.104>
63. Peng X, Liu D, Zhao F, Tang C (2022) Gas sensing properties of Mg-doped graphene for H₂S, SO₂, SOF₂, and SO₂F₂ based on DFT. *Int J Quantum Chem*. <https://doi.org/10.1002/qua.26989>
64. Gecim G, Ozekmekci M (2021) A density functional theory study of molecular H₂S adsorption on (4,0) SWCNT doped with Ge, Ga and B. *Surf Sci*. <https://doi.org/10.1016/j.susc.2021.121876>
65. Khodadadi Z (2018) Evaluation of H₂S sensing characteristics of metals-doped graphene and metals-decorated graphene: Insights from DFT study. *Phys E*. <https://doi.org/10.1016/j.physe.2018.02.022>
66. Fellah MF (2016) Adsorption of hydrogen sulfide as initial step of H₂S removal: A DFT study on metal exchanged ZSM-12 clusters. *Fuel Process Technol*. <https://doi.org/10.1016/j.fuproc.2016.01.003>
67. Fellah MF (2019) Pt doped (8,0) single wall carbon nanotube as hydrogen sensor: A density functional theory study. *Int J Hydrogen Energy*. <https://doi.org/10.1016/j.ijhydene.2019.08.169>
68. Ahmadi A, Hadipour NL, Kamfiroozi M, Bagheri Z (2012) Theoretical study of aluminum nitride nanotubes for chemical sensing of formaldehyde. *Sens Actuators B*. <https://doi.org/10.1016/j.snb.2011.12.001>
69. Hadipour NL, Peyghan AA, Soleymanabadi H (2015) Theoretical study on the Al-doped ZnO nanoclusters for CO chemical sensors. *J Phys Chem C*. <https://doi.org/10.1021/jp513019z>
70. Peyghan AA, Hadipour NL, Bagheri Z (2013) Effects of Al doping and double-antisite defect on the adsorption of HCN on a BC₂N nanotube: Density functional theory studies. *J Phys Chem C*. <https://doi.org/10.1021/jp312503h>
71. Eslami E, Vahabi V, Peyghan AA (2016) Sensing properties of BN nanotube toward carcinogenic 4-chloroaniline: A computational study. *Phys E*. <https://doi.org/10.1016/j.physe.2015.09.043>
72. Khan MS, Khan MS (2012) Comparative theoretical study of iron and magnesium incorporated porphyrin induced carbon nanotubes and their interaction with hydrogen molecule. *Phys E*. <https://doi.org/10.1016/j.physe.2012.05.010>
73. Utsu PM, Gber TE, Nwosa DO, Nwagu AD, Benjamin I, Ikot IJ, Eno EA, Offiong OE, Adeyinka AS, Louis H (2023) Modeling of anthranilhydrazide (HL1) salicylhydrazone and its copper complexes Cu(I) and Cu(II) as a potential antimicrobial and antituberculosis therapeutic candidate. *Polycyclic Aromat Compd*. <https://doi.org/10.1080/10406638.2023.2186444>
74. Sjoberg P, Politzer P (1990) Use of the electrostatic potential at the molecular surface to interpret and predict nucleophilic processes. *J Phys Chem*. <https://doi.org/10.1021/j100373a017>
75. Baydir E, Altun A, Fellah MF (2022) Molecular adsorption of silane on Ge, Ga and Al-doped CNT structures: a density functional theory study. *Prot Met Phys Chem Surf*. <https://doi.org/10.1134/S2070205122050033>
76. Johnson ER, Keinan S, Mori-Sánchez P, Contreras-García J, Cohen AJ, Yang W (2010) Revealing noncovalent interactions. *J Am Chem Soc*. <https://doi.org/10.1021/ja100936w>
77. Peng S, Cho K, Qi P, Dai H (2004) Ab initio study of CNT NO₂ gas sensor. *Chem Phys Lett*. <https://doi.org/10.1016/j.cplett.2004.02.026>

Publisher's Note Springer Nature remains neutral with regard to jurisdictional claims in published maps and institutional affiliations.

Springer Nature or its licensor (e.g. a society or other partner) holds exclusive rights to this article under a publishing agreement with the author(s) or other rightsholder(s); author self-archiving of the accepted manuscript version of this article is solely governed by the terms of such publishing agreement and applicable law.